Magnetic properties of $Y_2Fe_{14}B$ and $Nd_2Fe_{14}B$ and their hydrides

A. V. Andreev, A. V. Deryagin, N. V. Kudrevatykh, N. V. Mushnikov, V. A. Reĭmer, and S. V. Terent'ev

Ural State University

(Submitted 15 July 1985)
Zh. Eksp. Teor. Fiz. **90**, 1042–1050 (March 1986)

The effects of hydrogen on the magnetic moment, exchange interaction, magnetocrystalline anisotropy, and magnetostriction in $Y_2Fe_{14}B$ and $Nd_2Fe_{14}B$ and their hydrides are investigated, and the magnetic moment and Curie temperature are found to increase as hydrogen is absorbed. With decreasing temperature $T < 120$ K a spin reorientation is observed both in $Nd_2Fe_{14}B$ and in the hydride $Nd_2Fe_{14}BH_{3.8}$, which may be attributed to the different signs of the local anisotropy constants for the Nd ions at crystallographically inequivalent sites, and/or to the enhanced contribution of fourth-order anisotropy to the first anisotropy constant. The magnetization and longitudinal magnetostriction curves along the [100] and [110] directions contain discontinuities which correspond to first-order phase transitions induced by the magnetic field. Hydrogen absorption rapidly degrades the hysteresis magnetic properties of Nd-Fe-B magnets, which therefore cannot be used in hydrogen-enriched air.

There is much interest in the recently discovered class of rare-earth intermetallic compounds of the form $R_2Fe_{14}B$, because permanent magnets with unprecedentedly high energy products 290–341 kJ/m^3 can be fabricated from $Nd_2Fe_{14}B$ (Refs. 1–3). These materials readily absorb gaseous hydrogen at room temperature and pressure 10^5–10^6 Pa (Ref. 4). Since hydrogen absorption is accompanied by a rearrangement of the electron structure of the intermetallides and changes in the distances between the magnetoactive ions, it will be of interest to investigate how the absorbed hydrogen alters the magnetic properties. In the present work we study the magnetic moment, magnetocrystalline anisotropy, and magnetostriction in $Nd_2Fe_{14}B$, $Y_2Fe_{14}B$, and their hydrides; we also consider how hydrogen affects the hysteresis properties of sintered Nd-Fe-B permanent magnets.

EXPERIMENTAL METHOD

The $R_2Fe_{14}B$ compounds were prepared by melting the starting components [Nd (99.4%), Y (99.76%), Fe (99.99%), and B (96.4%)] in an induction oven in a helium atmosphere. Annealing yielding a coarse-grained bar, and spherical specimens of diameter 2–2.5 mm were obtained from individual grains. X-ray patterns were recorded from several faces of the crystals to verify that they were structurally perfect. In all specimens the subgrain misorientation angle was less than 3°. Permanent magnets were obtained by pulverizing the starting alloy and pressing the powder in a magnetic field, after which the material was sintered and then annealed.

The specimens were hydrated using gaseous hydrogen at room temperature and $p_H = 2 \cdot 10^5$ Pa as described previously in Ref. 5, and the hydrides $Nd_2Fe_{14}BH_{3.8}$ and $Y_2Fe_{14}BH_{4.8}$ were obtained. The lattice parameters for the starting and the hydrated materials are shown in Table I. The magnetic properties of the single crystals were studied by the induction method in pulsed magentic fields $\leqslant 16$ MA/m and on a vibrating magnetometer for $H \leqslant 1$ MA/m for temperatures between 4.2 and 700 K. The errors in measuring the magnetic moment by these two methods were equal to 5 and 3%, respectively. We used a quartz piezoelectric gage[6] to study the absolute magnetostriction in pulsed magnetic fields; these measurements were accurate to within 30%.

MAGNETIC MOMENT AND EXCHANGE INTERACTIONS

Figure 1 shows temperature curves for the molecular magnetic moments μ_m of single-crystal $Y_2Fe_{14}B$, $Nd_2Fe_{14}B$, and the corresponding hydrides. The curves were plotted from measurements of the specific magnetization along the easy [001] axis in 1 MA/m field. We see that hydration increased μ_m for both the Y and the Nd compounds, which is not surprising, since an increase in the magnetic moment μ_{Fe} of iron is generally observed when binary intermetallic compounds containing iron are hydrated.[7] The increase in μ_{Fe} is usually ascribed to the fact that in compounds containing iron, hydrogen creates low-energy electron states which are filled by electrons from the 3*d*-band. This is accompanied by a decrease in the Fermi energy and enhanced

TABLE I. Crystal lattice parameters and magnetic properties of $R_2Fe_{14}B$ compounds and their hydrides.

Compound	Lattice parameters		T_c, K	μ_m, μ_B/f.u.		K_1, 10^5 J/m^3	
	a,nm	*c*,nm		4.2 K	300 K	4.2 K	300 K
$Nd_2Fe_{14}B$	0.8801	1.2205	595	34.0	30.8	−57	49
$Nd_2Fe_{14}BH_{3.8}$	0.8919	1.2345	630	34.8	32.1	−57	7.9
$Y_2Fe_{14}B$	0.8754	1.2024	575	28.5	23.8	6.9	9.9
$Y_2Fe_{14}BH_{4.8}$	0.8830	1.2130	610	31.7	26.0	0.68	2.5

 0038-5646/86/030608-05$04.00

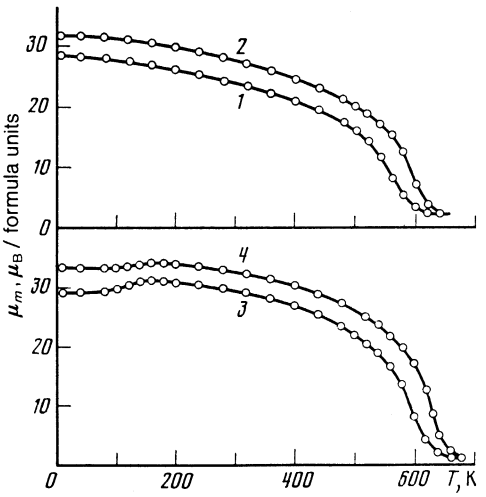

FIG. 1. Temperature dependence of the molecular magnetic moments along the c axis for $Y_2Fe_{14}B$ (1), $Y_2Fe_{14}BH_{4.8}$ (2), $Nd_2Fe_{14}B$ (3), and $Nd_2Fe_{14}BH_{3.8}$ (4).

splitting of the $3d$-band, which is responsible for the increase in μ_{Fe}. The situation in $R_2Fe_{14}B$ is apparently similar; however, because of the relatively low hydrogen content in this case, the 12% increase in μ_{Fe} is considerably less than the 25% reached in RFe_2 (Ref. 5).

Although hydration increases the interatomic distances, the Curie temperature is found to increase for both R = Y and R = Nd (cf. Table I), which indicates that the Fe-Fe exchange interaction must be enhanced. As was noted in Ref. 8, the structure $R_2Fe_{14}B$ and R_2Fe_{17} are closely related. Experiments on T_c as a function of an applied external pressure p (Ref. 9) revealed that for R_2Fe_{17}, T_c drops as p increases, i.e., as the interatomic distance decreases. A similar dependence of the exchange integral on the interatomic distance probably occurs in $R_2Fe_{14}B$.

The values of T_c in Table I for the hydrides are probably somewhat too low, because the hydrides $R_2Fe_{14}BH_x$ are thermodynamically unstable for $T > 500$ K and lose some of their hydrogen. Heating to 700 K removes the hydrogen almost completely, and to within the experimental error the temperature dependences of the magnetic moments are the same as for unhydrated specimens.

MAGNETOCRYSTALLINE ANISOTROPY

At room temperature $Nd_2Fe_{14}B$ and $Y_2Fe_{14}B$ are uniaxial ferromagnets with a [001] easy axis. However, in $Nd_2Fe_{14}B$ the easy axis deviates from the [001] axis as T increases.[2] Figure 2 shows some magnetization curves for the single crystals and hydrides along various crystallographic axes. By examining the projections of the spontaneous magentization on the [100], [110], and [001] crystallographic axes, we found that the magnetic moments for R = Nd lie in the (110) plane for $T = 4.2$ K and make an angle of 26° with the [001] axis for $Nd_2Fe_{14}B$ (28° for the hydride). The $\sigma(H)$ curves along the [001] and [110] directions exhibit discontinuities at certain critical fields; they apparently correspond to a first-order phase transition induced by the magnetic field.

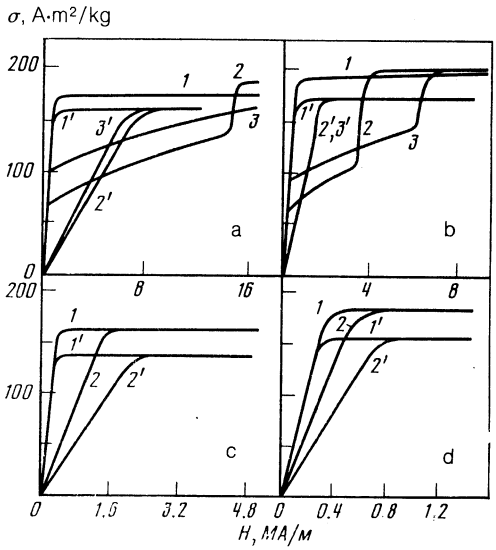

FIG. 2. Magnetization curves for single-crystal $Nd_2Fe_{14}B$ (a), $Nd_2Fe_{14}BH_{3.8}$ (b), $Y_2Fe_{14}B$ (c), and $Y_2Fe_{14}BH_{4.8}$ (d) along several crystallographic directions: [001] (1), [100] (2), [110] (3) ($T = 4.2$ K); [001] (1'), [100] (2'), [110] (3') ($T = 300$ K).

The compounds $R_2Fe_{14}B$ have a tetragonal crystal lattice belonging to the space group $P4_2/mnm$ with 68 atoms per unit cell (4 formula units).[10] There are two inequivalent rare-earth sites, 6 inequivalent sites for Fe, and only one site for B. If we neglect anisotropy constants of order $\geqslant 6$, the anisotropy energy of a tetragonal crystal can be expressed in the form

$$E_a = K_1 \sin^2\theta + K_2 \sin^4\theta + K_3 \sin^6\theta + K_4' \sin^4\theta \cos 4\varphi + K_6' \sin^4\theta (11\cos^{-2}\theta - 1)\cos 4\varphi. \quad (1)$$

Here θ is the angle between the magnetization vector **M** and the [001] axis, and φ is the angle between the [110] axis and the projection of **M** onto the basis plane. An analytic expression for the magnetization along the [110] axis follows by minimizing the free energy

$$F = E_a - M_s H \sin\theta\cos\varphi + {}^1/_2 N M_s^2 \sin^2\theta\cos^2\varphi, \quad (2)$$

where M_s is the saturation magnetization and N is the demagnetization factor. For the special case when M rotates in the (110) plane, i.e., $\varphi = 0$, we have

$$\frac{H}{j} = \left(\frac{2K_1}{M_s} + NM_s\right) + \frac{4(K_2 + K_4' + 10K_6')}{M_s} j^2 + \frac{6(K_3 - 11K_6')}{M_s} j^4, \quad (3)$$

where we have written $j = \sin\theta = M(H)/M_s$.

Equation (3) describes a parabola when plotted in the $H/j, j^2$ plane. We can use Eq. (3) to approximate the experimental magnetization curves along the [110] axis and calculate some of the anisotropy constants. For $Nd_2Fe_{14}B$ and $Nd_2Fe_{14}BH_{3.8}$, the jumps in the magnetization combined with the low measurement accuracy make it impossible to determine all of the coefficients multiplying the powers of j in (3). We found the anisotropy constants

$$K_1 \text{ and } K_2^{\text{eff}} = K_2 + K_4' + 10K_6'$$

by extrapolating the dependence $H/j(j^2)$ to $j = 0$. Their

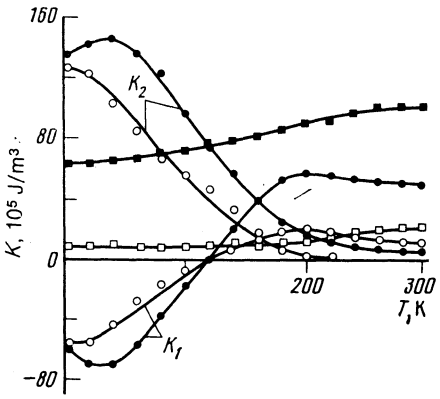

FIG. 3. Temperature dependences of the anisotropy constants K_1 and K_2^{eff} for $Nd_2Fe_{14}B$ (●) and $Nd_2Fe_{14}BH_{3.8}$ (○), and $K_1 \times 10$ for $Y_2Fe_{14}B$ (■) and $Y_2Fe_{14}BH_{4.8}$ (□).

temperature dependences are shown in Fig. 3, which also gives $K_1(T)$ for $Y_2Fe_{14}B$ and $Y_2Fe_{14}BH_{4.8}$.

The high uniaxial anisotropy of the iron sublattice in $Y_2Fe_{14}B$ and the anomalous increasing temperature dependence $K_1(T)$ are striking; they probably reflect competition among the local anisotropies of the Fe ions at the six inequivalent lattice sites and differences in their temperature behavior. The high anisotropy of the Fe sublattice is apparently caused by partial "unfreezing" of the orbital momentum of the Fe ions and by their interaction with the crystal field of the lattice, as occurs for Co ions in certain compounds.[11] A high magnetocrystalline anisotropy in the Fe ion sublattice was previously noted[12] for R_2Fe_{17} compounds with a related crystal structure.

Since at room temperature K_1 is greater for the Nd compounds than for Y, competition between the contributions from the Fe and Nd sublattices to the anistropy cannot account for the spin reorientation. The nonmonotonic behavior of K_1 could be due to the different signs of the (large) local anisotropy contants of the Nd ions at inequivalent sites. In this case a noncollinear magnetic structure is produced and the spin reorientation could result from the different temperature dependences of the local anisotropy constants, or it could come about because the anisotropy energy of the Fe ion sublattice decreases faster than the exchange energy as T increases, so that there is a transition to a collinear magnetic structure.

The sign of the single-ion local anisotropy constant associated with the interaction between the 4*f*-electron cloud and the crystal field is known[13] to depend on the sign of the Elliot-Stevens parameters, which depends on the shape of the 4*f*-electron cloud, and on the crystal field parameters A_{nm}, which in the point charge model are given by

$$A_{nm}^{(i)} = Z_i \lambda_{nm}(i), \tag{4}$$

where Z_i is the effective charge of ions at the ith lattice site, and the lattice sums λ_{nm} are defined by

$$\lambda_{nm} = \left(\frac{4\pi}{2n+1}\right)^{1/2} \sum_k \frac{1}{R_k^{n+1}} Y_n^m(\theta_k, \varphi_k). \tag{5}$$

Here R_k is the distance from an atom at the k-*th* site, and the $Y_n^m(\theta_k, \varphi_k)$ are spherical harmonics. Table II lists the nonzero sums λ_{nm} for the two inequivalent Nd lattice sites; the radius of summation is equal to 0.5 nm. The interatomic distances and atomic coordinates in the lattice needed in the calculations were taken from Ref. 10. In addition to the values shown in Table II, the local anisotropy of each Nd atom also contains contributions from the imaginary parts of the lattice sums λ_{22} and λ_{42}; however, their total contribution over the entire crystal vanishes due to the lattice symmetry.

The effective charges of the ions must be specified before one can calculate the magnitudes and sign of the parameters A_{nm}. It was shown in Refs. 13 and 14 that for many intermetallic compounds, the point charge model gives anisotropy coefficients in best argreement with experiment if one assumes an effective charge of $\approx 3^+$ for the rare-earth ion and a positive but very small charge for Fe. If we assume that $1 < Z_R < 3$ in $Nd_2Fe_{14}N$ and $0 < Z_{Fe} < 1$, then if $Z_R > 1.4 Z_{Fe}$ one can always choose B-ion charges in the interval $-4.3 < Z_B < 2.1$, in which the crystal field parameters A_{20} have different signs for Nd at the inequivalent sites—A_{20} is negative in the 4*f* position but positive at the 4*g* site. A nonmonotonic dependence $K_1(T)$ for $Nd_2Fe_{14}B$ caused by the opposite signs of the anisotropy coefficients for the two Nd sublattices is thus consistent with the point charge model.

However, another interpretation is also possible. According to Ref. 14, for uniaxial crystals the anistropy constants in (1) are related by

$$K_1 = -{}^3/_2 K_2^0 - 5K_4^0, \quad K_2 = {}^{35}/_8 K_4^0 \quad \text{or} \quad K_2^0 = -{}^2/_3 (K_1 + {}^8/_7 K_2),$$
$$K_4^0 = {}^8/_{35} K_2 \tag{6}$$

to the expansion coefficients of the anisotropy as a series in the spherical harmonics (we neglect coefficient of order $\geqslant 6$). Because the experimental values of K_2 for $Nd_2Fe_{14}B$ are large and positive but decrease rapidly as T increases, the negative values of K_1 at low temperature could reflect a large contribution of K_4^0 to K_1. The points in Fig. 4 show $K_2^0(T)$ and $K_4^0(T)$ calculated from the experimental curves K_1 and K_2 for hydrated and unhydrated $Nd_2Fe_{14}B$. The solid curves give the temperature dependences for $K_l^0(T)$ calculated using the single-ion model[15]:

$$K_l^0(T) = K_l^0(0) L_l^J(gJ\mu_B H_m / K_B T). \tag{7}$$

The experimental and calculated values K_4^0 agree best if one takes $H_m = 2.7 \times 10^8$ A/m and $2.0 \cdot 10^8$ A/m for the effective

TABLE II. Lattice sums for $Nd_2Fe_{14}B$.

Positions	Total contribution from Nd atoms			Total contribution from Fe atoms			Total contribution from all B atoms		
	λ_{20}, $10\ \text{nm}^{-3}$	λ_{40}, $10^2\ \text{nm}^{-5}$	λ_{44}, $10^2\ \text{nm}^{-5}$	λ_{20}, $10\ \text{nm}^{-3}$	λ_{40}, $10^2\ \text{nm}^{-5}$	λ_{44}, $10^2\ \text{nm}^{-5}$	λ_{20}, $10\ \text{nm}^{-3}$	λ_{40}, $10^2\ \text{nm}^{-5}$	λ_{44}, $10^2\ \text{nm}^{-5}$
4*f*	−2.937	1.609	−0.436	8.438	−5.492	1.024	−2.046	1.821	−2.540
4*g*	−1.824	0.948	0.486	8.649	−4.974	−2.277	−2.902	2.056	1.131

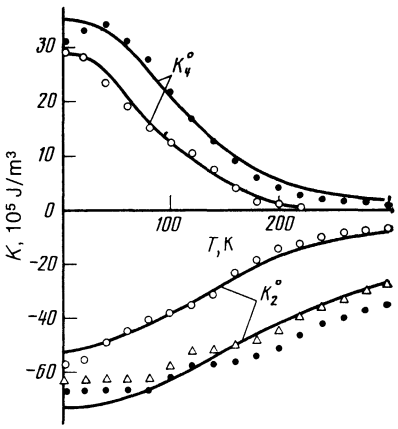

FIG. 4. Temperature dependences of the anisotropy coefficients K_2^0 and K_4^0 for $Nd_2Fe_{14}B$ (●, △) and $Nd_2Fe_{14}BH_{3.8}$ (○). The solid curves were calculated using the single-ion model.

field exerted on the Nd sublattice by the Fe sublattice for unhydrated and hydrated $Nd_2Fe_{14}B$, respectively. We used these effective fields to calculate the temperature dependences of the coefficients K_2^0; the calculated values of K_2^0 for the hydride agree satisfactorily with experiment, but $K_2^0(T)$ for $Nd_2Fe_{14}B$ differs considerably from the dependence predicted by the single-ion model. Much better agreement is obtained if we include the contribution to K_2^0 from the Fe sublattice. The triangles in Fig. 4 show the corrected values

$$(K_2^0)_{Nd} = (K_2^0)_{Nd_2Fe_{14}B} - {}^2/_3 (K_1)_{Y_2Fe_{14}B}.$$

Since the magnetic anisotropy in the hydride $Y_2Fe_{14}BH_{4.8}$ is much less than for $Y_2Fe_{14}B$, the contribution from the iron sublattice may be neglected in this case.

In addition to explaining the spin reorientation in the Nd compounds, this approach can also be used to estimate the interlattice exchange interaction field in these materials. However, it has the drawback of neglecting the higher-order anisotropy constants K_3 and K_6, which are essential in describing the discontinuities of the magnetization.

MAGNETOSTRICTION

Figure 5 shows the field dependence of the longitudinal magnetostriction $\lambda_{\parallel}(H)$ at 4.2 and 300 K. We see that for H less than the anisotropy field H_A, $\lambda_{\parallel}$ for the Y compounds is roughly proportional to the square of the magnetization, while for $H > H_A$ there is considerable paramagnetic magnetostriction, which is probably caused by the strong dependence of the exchange integral $J_{Fe\text{-}Fe}$ on the interatomic distance (a similar conclusion was reached in Ref. 16, where the lattice parameters for these compounds were measured as a function of temperature).

We conclude by comparing the $\lambda(H)$ curves for compounds containing Y and Nd that at room temperature, rotation of the magnetic moment of the Fe sublattice is primarily responsible for the anisotropic magnetostriction in $Nd_2Fe_{14}B$ and its hydride; however, at low temperatures the Nd sublattice gives a comparable contribution to λ. If M deviates only slightly from the [001] easy axis, this contribution is negative and smaller in absolute value than λ_{Fe} in

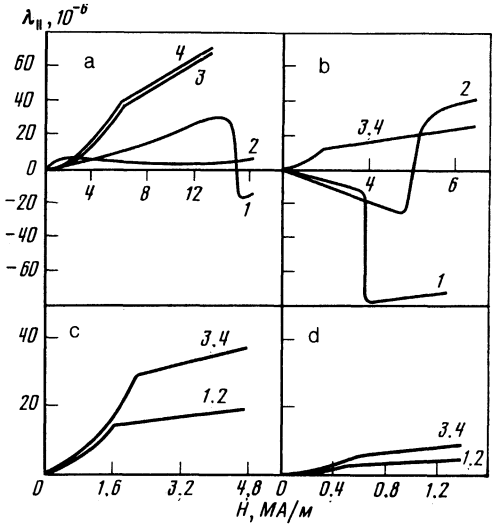

FIG. 5. Field dependences of the longitudinal magnetostriction $\lambda_{\parallel}$ for single-crystal $Nd_2Fe_{14}B$ (a), $Nd_2Fe_{14}BH_{3.8}$ (b), $Y_2Fe_{14}B$ (c), and $Y_2F_{14}BH_{4.8}$ (d) along various crystallographic directions: [100] (1), [110] (2) ($T = 4.2$ K); [100] (3), [110] (4) ($T = 300$ K).

$Nd_2Fe_{14}B$, but larger than λ_{Fe} for the hydride. The magnetostrictive deformation in $Nd_2Fe_{14}B$ and in $Nd_2Fe_{14}BH_{3.8}$ thus have opposite signs in fields up to 4 MA/m. Near the first-order magnetic phase transition, the magnetostriction curves have discontinuities of opposite signs for the [100] and [110] directions.

The widely used expression derived by Clark *et al.*[17] for the magnetostriction in a uniaxial crystal cannot be used to analyze our magnetostriction curves because of the pronounced anisotropy of the magnetostriction in the basis plane. A more refined theory is thus needed to describe the magnetoelastic interactions in compounds of the type $R_2Fe_{14}B$.

HYSTERESIS PROPERTIES

In applications, permanent magnets may be exposed to gaseous hydrogen or come in contact with acids and absorb hydrogen by electrolysis. It will therefore be of interest to examine how hydrogen alters the mechanical and magnetic properties of $Nd_2Fe_{14}B$ permanent magnets.

Sintered permanent magnets absorb hydrogen just as readily as the starting alloy, and absorption is accompanied by considerable embrittlement. Figure 6 shows some magnetic characteristics for an Nd-Fe-B permanent magnet with a maximum specific magnetic energy $(BH)_m = 270$ kJ/m^3 at room temperature; the corresponding curves for the same magnet after hydration are also shown. Just as in the case of single crystals, hydrogen absorption increases the specific magnetization, but the anisotropy and coercive fields H_A and H_c are greatly decreased (the anisotropy field for a permanent magnet is the minimum field required to saturate the magnetization curves normal to the axis of the texture). Although adding hydrogen can in theory increase the maximum energy product, in practice this does not occur due to the smallness of H_c. Hydrogen absorption thus degrades the performance of permanent $Nd_2Fe_{14}B$ magnets.

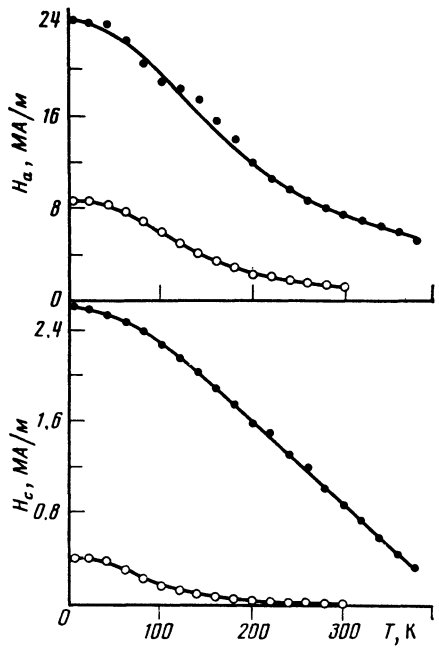

FIG. 6. Temperature dependences of the anisotropy and coercive fields H_A, H_C for an Nd-Fe-B permanent magnet before (●) and after (○) hydration.

CONCLUSIONS

Our studies show that hydration of $R_2Fe_{14}B$ compounds increases the magnetic moment of the iron sublattice and decreases the magnetic anisotropy. The spin-flip transition at low temperatures for compounds with R = Nd is due partly to the different signs of the local anisotropy constants for Nd ions at inequivalent lattice sites, and partly to the large contribution to K_1 from the fourth-order anisotropy. For specimens magnetized along the [100] and [110] axes, the magnetization and magnetostriction curves have discontinuities which can be interpreted as field-induced first-order magnetic phase transitions. Because it reduces the anisotropy field and makes the materials brittle, hydrogen absorption seriously degrades the properties of permanent $N_2Fe_{14}B$ magnets.

[1]M. Sagawa, S. Fujimura, N. Togawa, H. Yamamoto, and Y. Matsuura, J. Appl. Phys. **55**, 2083 (1984).
[2]A. V. Deryagin, E. N. Tarasov, A. V. Andreev, V. N. Moskalev, and A. I. Kozlov, Pis'ma Zh. Eksp. Teor. Fiz. **39**, 516 (1984) [JETP Lett. **39**, 629 (1984)].
[3]A. L. Robinson, Science 223, 920 (1984).
[4]K. Oesterreicher and H. Oesterreicher, Phys. Status Solidi (a) **85**, K61 (1984).
[5]A. V. Deryagin, V. N. Moskalev, N. V. Mushnikov, and S. V. Terent'ev, Fiz. Met. Metalloved. **57**, 1086 (1984).
[6]V. V. Snegirev, Candidate's Dissertation, Moscow (1984).
[7]K. H. J. Buschow, Solid State Commun. **19**, 421 (1976).
[8]J. F. Herbst, J. J. Croat, F. E. Pinkerton, and W. B. Yelon, Phys. Rev. B **29**, 4176 (1984).
[9]M. Brouha and K. H. J. Buschow, J. Appl. Phys. **44**, 1813 (1973).
[10]D. Givord, H. S. Li, and J. M. Moreau, Solid State Commun. **50**, 497 (1984).
[11]R. L. Streever, Phys. Rev. B **19**, 2704 (1979).
[12]A. V. Deryagin and N. V. Kudrevatykh, in: All-Union Conf. Phys. Magn. Phen., Khar'kov (1979), p. 445.
[13]A. A. Kazakov and V. A. Reĭmer, Fiz. Met. Metalloved. **51**, 530 (1981).
[14]N. V. Kudrevatykh, A. V. Deryagin, A. A. Kazakov, V. A. Reĭmer, and V. N. Moskalev, Fiz. Met. Metalloved. **45**, 1169 (1978).
[15]A. A. Kazakov and R. I. Andreeva, Fiz. Tverd, Tela **12**, 240 (1970) [Sov. Phys. Solid State **12**, 192 (1970)].
[16]A. V. Andreev, A. V. Deryagin, S. M. Zadvorkin, and S. V. Terent'ev, Fiz. Tverd, Tela **27**, 1641 (1985) [Sov. Phys. Solid State **27**, 987 (1985)].
[17]A. E. Clark, B. F. Desavage, and R. Bozorth, Phys. Rev. **138**, A216 (1965).

Translated by A. Mason